Int. J. Appl. Ceram. Technol., 12 [1] 26–31 (2015)
DOI:10.1111/ijac.12306

Thermoplastic 3D Printing—An Additive Manufacturing Method for Producing Dense Ceramics

Uwe Scheithauer,* Eric Schwarzer, Hans-Jürgen Richter, and Tassilo Moritz

Fraunhofer Institute for Ceramic Technologies and Systems IKTS, Dresden 01277, Germany

In our new approach—thermoplastic 3D printing—a high-filled ceramic suspension based on thermoplastic binder systems is used to produce dense ceramic components by additive manufacturing. Alumina (67 vol%) and zirconia (45 vol%) suspensions were prepared by ball milling at a temperature of about 100°C to adjust a low viscosity. After the preparation the suspension solidified at cooling. For the sintered samples (alumina at 1600°C, zirconia at 1500°C), a density of about 99% and higher was obtained. FESEM studies of the samples' cross section showed a homogenous microstructure and a very good bond between the single printed layers.

Introduction

Today, additive manufacturing (AM) of polymers is state-of-the-art, see for example.[1,2] In the field of metals, more and more materials can be processed as well.[3] For producing ceramic components, the technical application of AM technologies is yet limited. However, ceramic materials have been studied in additive manufacturing processes ab initio with the development of the different AM technologies since about 25 years, see for example.[4,5] All popular AM technologies—formerly referred as rapid prototyping (RP) or solid free form fabrication (SFF)—have been tested also for ceramic materials, which are shown subsequently.

The conventional stereolithography (STL) process, for example, was applied for alumina,[6] silicon nitride, and silica[7] as well as for ZTA.[8] In this STL-process, a photopolymerizable ceramic suspension is cured by an UV-laser. Based on the principal approach of using light-curable binders in the ceramic suspension or paste, specific AM techniques for the production of ceramic green bodies have been developed. So, UV curable inks with high Al_2O_3 loading are used in a robocasting process.[9] Binders that are cured under visible blue light are applied in a DLP (direct light processing) process, which allows to produce complex-shaped dense alumina parts.[10]

Selective laser sintering (SLS) and 3D powder bed printing are typical AM powder-based processes. SLS was tested for a number of ceramic materials.[11–15] A typical application of 3D powder bed printing is focused on the production of porous ceramic components because of the powder layers, which are not compacted, and the green density is too low to reach high density (>99%) after sintering. However, high densities are not required, for example for bioactive scaffold structures. So, complex individual bioactive components based on calcium phosphates have been produced by 3D powder bed printing.[16–20] Another way to utilize the relative simple 3D-powder bed printing technique is the infiltration of the 3D printed and sintered porous ceramic component with liquid metal that was shown in.[21] It is also possible to use a ceramic particle-filled ink in powder bed printing to adjust the composition and the green density of the printed sample.[22]

In general, when using AM methods for production of samples with high sinter density, it is necessary to use a suspension with a high powder volume content instead of a dry powder bed. This was shown, for example, in SLS process at which instead of powder layers a suspension layers were deposited and consolidated (after short drying) by laser beam.[23]

The direct printing of suspensions is not only applied in combination with powder bed printing. High-filled ceramic suspensions have been also processed by direct ink-jet printing to fabricate complex-shaped ceramic components.[24]

The conventional fused deposition modeling (FDM) uses a thermoplastic ceramic feedstock that is liquefied by heating and pressed through a fine nozzle—that means, in the physical sense a suspension is used too. For example, functional ceramic materials[25] and alumina[26] were processed using FDM. However, the efforts for the preparation of the thermoplastic ceramic feedstock in the form of spooled filaments constrain the FDM application for ceramics.

The robocasting process which is a computer-controlled deposition of colloidal pastes or slurries is similar

*uwe.scheithauer@ikts.fraunhofer.de

to FDM. In contrast to original FDM and other generative extrusion processes, the carrier fluid is a volatile solvent (water or organic liquid). In robocasting, highly dispersed ceramic suspensions are used for AM of complex ceramic structures.[27–29]

Our approach combines FDM and robocasting. We use thermoplastic binder systems to prepare highly loaded feedstocks that are processed in a heatable dispensing unit with xyz positioning. The thermoplastic feedstocks are based on compositions that known from low-pressure injection molding.[30,31] The melting temperature is relatively low (approx. 100°C) and the viscosity is also relatively low as compared to typical thermoplastic feedstocks for high-pressure injection molding. So, the liquid feedstock (=suspension) cannot only be simply dispensed via a thin nozzle as nearly endless filament which is similar to FDM and robocasting but also discontinuous as droplets by micro-dispensing technology, which allows the realization of very fine structures with smaller tolerances. The heated suspension is printed layer by layer. The suspension immediately solidifies due to cooling because of the fast heat transfer from the printed suspension to the underlying layer or to the surrounding atmosphere. The present paper shows the principle of this 3D thermoplastic printing as well as the results for alumina and zirconia.

Particularly In this paper, tests are described and discussed showing which sinter densities were achieved, which microstructures were developed, which rheological behavior the suspensions had and how the different layers were connected to each other.

Experimental Procedure

The AM laboratory equipment uses a xyz-actuating unit with a cartridge fitting. The cartridge can be moved in xyz direction above a fixed platform. For the experiments, a heated cartridge and fitting dosage needles were used to print the suspension on a metal tape or a glass slide as substrate (Fig. 1). The uniform heating of the cartridge, suspension as well as needle is very important as the viscosity of the suspension strongly depends on the temperature. The used needles had an inner diameter of 0.4 mm and 0.8 mm, and the heated suspension was deposit as continuous filament.

An extra cooling of the platform is not needful. At room temperature, the suspension solidifies immediately after printing on the substrate.

We used two different materials (alumina and zirconia) with different particle size distributions resulting in different realizable powder contents.

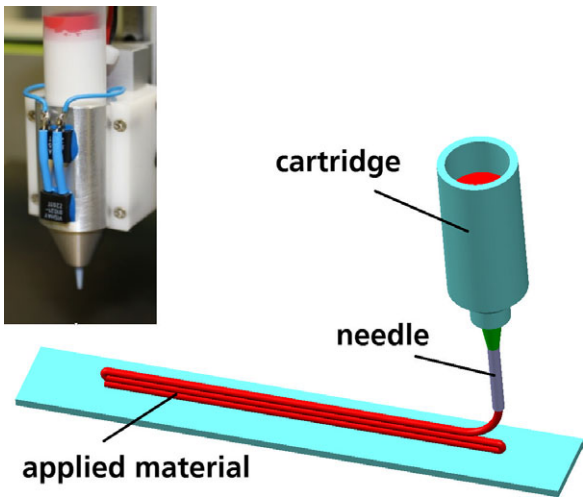

Fig. 1. Picture and scheme of the test equipment.

An alumina suspension (powder content 67 vol%) was prepared using alumina powder MR52 (Martinswerk, Bergheim, Germany) with d_{50} = 1–1.7 µm and a purity of 99.8 wt% Al_2O_3. As binder system, a mixture of paraffin and beeswax was used. The binder system and a dispersing agent were heated up to 100°C in a heatable ball mill. Then, the alumina powder was added to the liquid. The alumina suspension was prepared by ball milling at 100°C for 72 h.

For preparing a zirconia suspension (powder content 45 vol%), zirconia powder TZ-3Y-SE (Tosoh, Tokyo, Japan) with d_{50} = 0.3 µm and 94.5 wt% ZrO_2 was used. The partially stabilized ZrO_2 contains 3 mol% Y_2O_3. The lower powder content results from the smaller particles and the ten times higher specific surface of the zirconia compared with the used alumina.

The rheological characterization is very important to evaluate the processability of the suspension to estimate if it is possible to meter small volumes and which technologies can be used. Differences between the materials such as morphology and particle diameter influence the handling and processing and can be characterized by the rheological behavior.

An ideal suspension should have a pseudoplastic behavior in a low viscosity range. Viscoelastic behavior means that the suspension has a very low viscosity at high shear rates, which is important for metering small volumes through small geometries at low pressures, and that it has a high viscosity at low shear rates to be fixed at the point of application.

The flow behavior depends on different factors, for example temperature and material structure. For our process, it is essential to optimize this parameter because the

realizable resolution strongly depends on the metering (e.g., pressure), which in turn depends on the viscosity.

To characterize the rheological behavior of the alumina and the zirconia suspensions, a rheometer (Modular Compact Rheometer MCR 302; Anton Paar, Graz, Austria) adjustable between −25 to 200°C with a plate/plate measuring system was used. The flow behavior was analyzed with an increasing shear stress (0–2000 Pa) and at varying temperatures between 80°C and 120°C. The shear rate was measured. The graphic analyses were commonly performed, that means viscosity in dependence on shear rate.

The suspension was heated up to a temperature of about 80°C. A needle with a diameter of 0.8 mm was used and a pressure of 0.4 bar had to be applied to press the suspension out of the needle. If plastic needles were used, the temperature of the suspension decreased tremendously within the needle and the viscosity of the suspension was increased resulting in clogging of the needle. Using metal needles with a good thermal conductivity, the energy of the heated suspension inside the cartridge was also conducted to the top of the needle and clogging could be avoided.

Simple structures were produced which consisted of a number of different filaments on top of each other. The velocity of the moved needle was 20 mm/s.

The samples were debinded in a powder bed at very low heating rate under air and then sintered under air at a temperature of 1600°C (2 h) for alumina or 1350/1500°C (2 h) for zirconia. The sinter mechanism for both materials is solid-state sintering,[32,33] and dense microstructures could be reached with pressureless sintering.[34]

To evaluate the density of the sintered samples, Archimedes' principle and FESEM images were used. The FESEM images were converted into binary images, and all pores were converted into black pixels and the ceramic particles into white pixels. The used open source software is called Image J, National Institutes of Health, Bethesda, MD. The software compares the number of black and white pixels and calculates the porosity in the cross-sectional area.

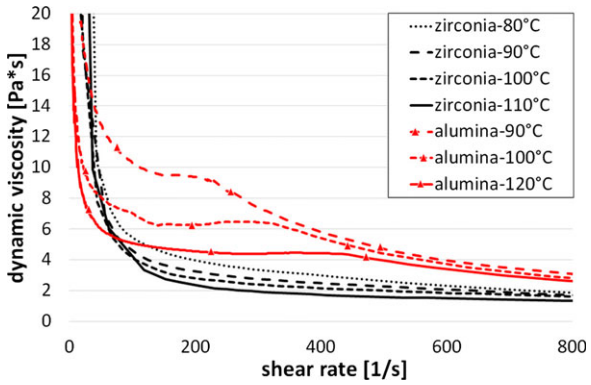

Fig. 2. Dynamic viscosity of alumina (67 vol%) and zirconia (45 vol%) suspensions plotted over the shear rate.

Results and Discussion

Figure 2 shows the flow curves of the alumina and zirconia suspensions at the various temperatures.

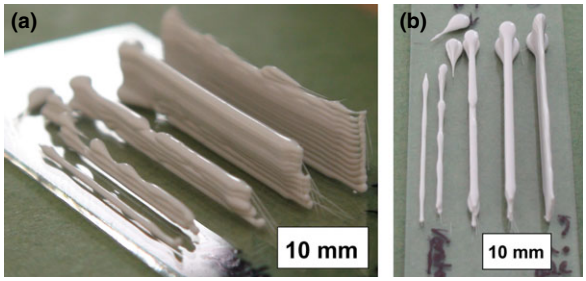

Fig. 3. Applied Al_2O_3 filaments: (a) overview; (b) topview.

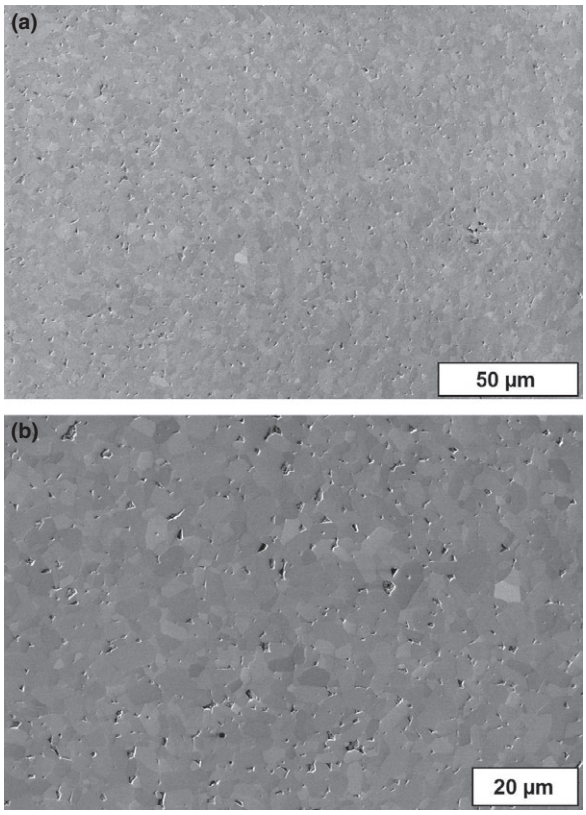

Fig. 4. FESEM images of cross section of Al_2O_3 sintered at 1600° C: (a) overview and (b) detail.

Independent of the material and of the temperature, the suspensions show a pseudoplastic behavior. The dynamic viscosity decreases with increasing temperature and increasing shear rate. That means, the suspensions remain without a deformation force at their shape. For the processing using the described shaping process, this behavior is an important factor. The suspension can flow at high shear rates induced by pressure and after the forming it is fixed on a defined position. Furthermore, if the temperature is increased, lower shear rates and pressures are required to reduce the viscosity. In general, alumina suspensions with a higher solid content of 67 vol% show a higher viscosity compared with the zirconia suspensions with a solid content of 45 vol%.

For alumina suspensions, the viscosity decreases significantly more with an increasing temperature at low shear rates between 0 and 400/s than at higher shear rates. For the used zirconia suspension, the dependence of the viscosity in this field of temperature is small and thereby the influence on the process as well.

Summarizing the rheological research shows that the developed process is working with different material systems, because the viscosity of the suspensions decreases to values between 2 and 5 Pa × s (shear rate higher than 50/s). This is important to produce structures with a high resolution. Furthermore, the curves help to examine

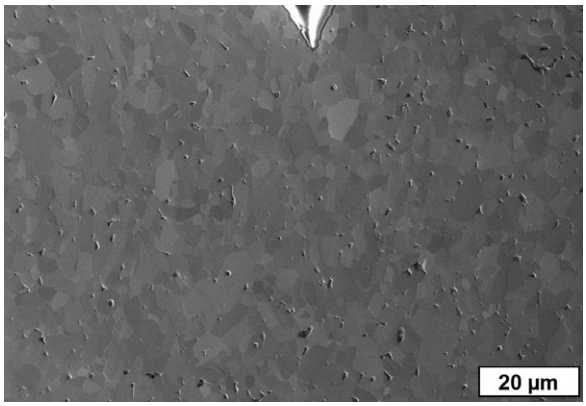

Fig. 6. FESEM images of cross section of Al_2O_3: very good bonding between the layers, grain growing across the interface.

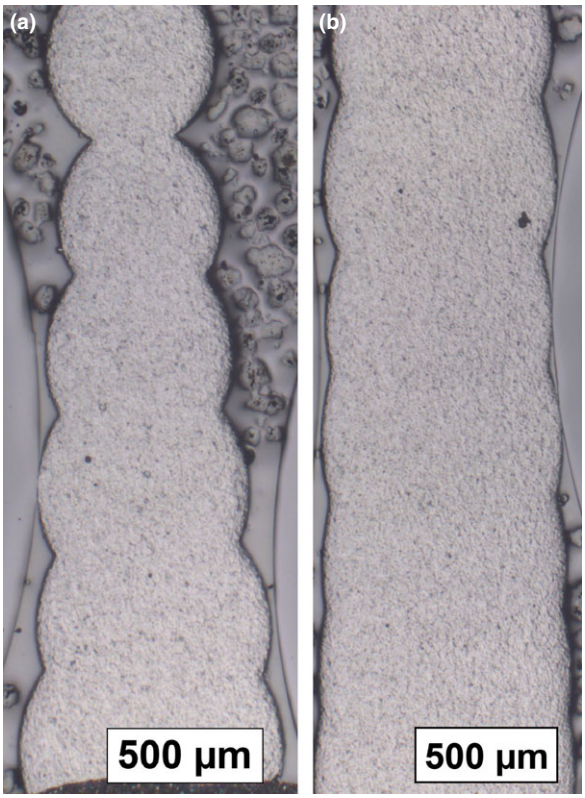

Fig. 5. Light microscopy images of cross section of seven Al_2O_3 layers on top of each other: (a) hardly deformed because of fast solidification; (b) a little deformed resulting in a smoother surface.

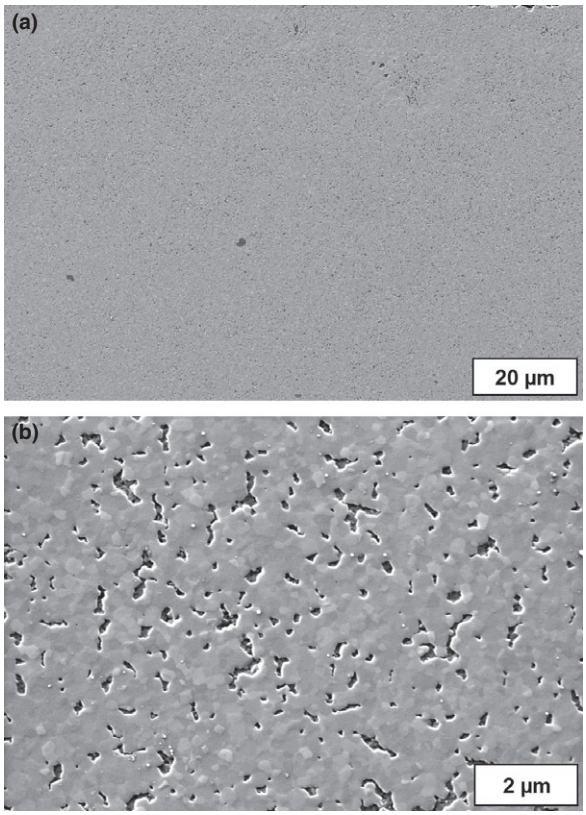

Fig. 7. FESEM images of cross section of ZrO_2 sintered at 1350° C, still high porosity, very small grains: (a) overview; (b) detail.

essential parameters (temperature; solid content) to handle the process in an optimal range.

Figure 3a and b show the produced alumina samples. More than ten different layers could be placed on top of each other without any deformation like the shifting of a layer. A very good bond between the different layers could be seen. Only at the starting point, too much material was applied, the material did not cool fast enough, and the structure deformed before it has solidified.

Figure 4a and b show FESEM images of cross section of Al_2O_3 sintered at 1600°C.

The density of nine alumina samples was measured using the Archimedes' principle. A density mean value of 97.3% of the theoretical density (3.96 g/cm^3) with a standard deviation of 0.8% of T.D. was calculated.

For 23 FESEM images of alumina samples, a mean porosity of 0.8 ± 0.4% was calculated. The mean grain size, estimated from the FESEM images, was about 6.5 μm because of the big size of the used particles (d_{50} = 1– 1.7 μm).

Figure 5a and b show light microscopy images of the alumina samples. The cross sections of the different filaments could be distinguished very well by the outer geometry, but not by a special interface between the layers. In the homogenous microstructure, an interface between the single printed layers is not visible (Fig. 6). There is a complete bond between the layers, grain growth occurred across the interface and layer separation was impossible.

The Figs 7 and 8 show FESEM images of cross sections of zirconia samples sintered at 1350°C (Fig. 7a,b) or 1500°C (Fig. 8a,b) for 2 h. The samples sintered at the lower temperature show a higher porosity and smaller grains.

For one sample sintered at 1350°C, an inner density of 5.7 g/cm^3 and an outer density of 4.9 g/cm^3 were measured by Archimedes' principle, which means an open porosity of about 14%. The optical investigation of FESEM images of eleven images of different samples showed a mean porosity of 5.6 ± 1.1%. The estimated mean grain size was 0.46 μm.

The other samples sintered at 1500°C had a very dense microstructure. The porosity measured by Archimedes' principle was about 2%. The optical investigation of eight images of different samples showed a mean porosity of 0.03 ± 0.02%. The estimated mean grain size was 0.96 μm.

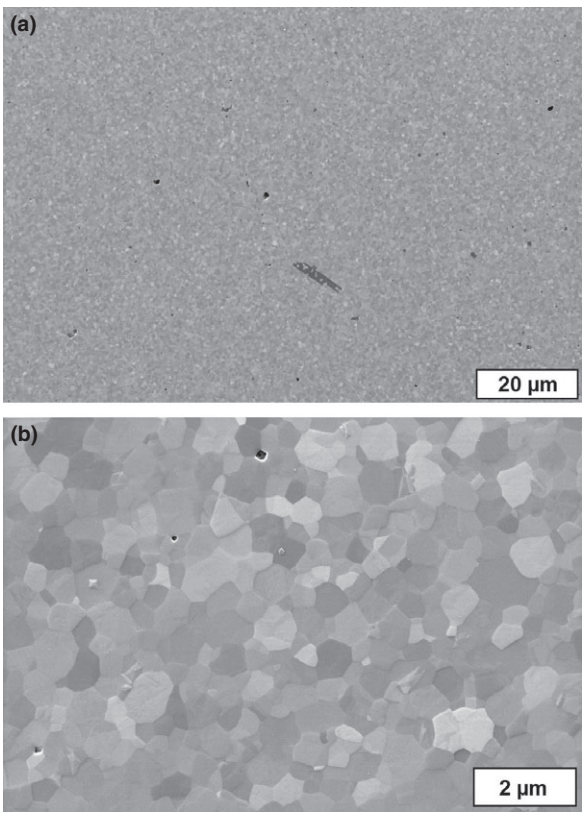

Fig. 8. FESEM images of cross section of ZrO_2 sintered at 1500° C, nearly no porosity, grains visible: (a) overview; (b) detail.

Summary and Conclusion

Thermoplastic 3D printing based on high-filled ceramic suspensions with thermoplastic binder systems is an interesting alternative additive manufacturing method to produce dense ceramics. For alumina and for zirconia, it was shown that

1. Thermoplastic suspensions with very high solid loading of Al_2O_3 or ZrO_2 can be prepared.
2. The viscosity varied in a range of about 5–10 Pa × s for shear rates between 50 and 100/s, which enables printing thru thin needle at low pressure.
3. Layers can be deposited on the top of each other with high edge stability.
4. Homogenous microstructure with very good bonding between the single printed layers is reached.
5. Very high densities of 99% and more are achieved for alumina and zirconia samples.

The low viscosity allows not only the pressing thru a needle but also high-quality dispensing technologies to form small droplets and to improve the possible resolution in all three directions of space.

Thermoplastic 3D printing has advantages over other suspension-based technologies like the use of photopolymerizable binders.

- The green layer is solidified by simple cooling.
- The method works almost independently from the (optical) properties of the ceramic material.
- The portfolio of applicable materials is not limited.
- The material can be applied on selected areas in a layer and does not have to be applied on the whole surface.

This opens a big field for application such as

- additive manufacturing of multimaterial and multifunctional components or the
- realization of material and/or property gradients in three dimensions.

But there are some challenges to cope with

- Heating rates for thermal debinding must be very low and it must be carried out in a powder bed.
- Abrasion of the equipment components is very high because of the highly loaded suspensions.

Acknowledgments

The authors want to thank Mr. Stockmann and Mr. Bedrich for the provision of the thermoplastic suspensions as well as Mrs. Jungnickel and Mrs. Fischer for the metallographic specimen preparation and the FESEM images.

References

1. M. Hofmann, *ACS Macro Lett.*, 3 [4] 382–386 (2014).
2. R. D. Goodridge, C. J. Tuck and R. J. M. Hague, *Prog. Mater. Sci.*, 57 [2] 229–267 (2012).
3. L. E. Murr, *et al.*, *J. Mater. Res.Technol.*, 1 [1] 42–54 (2012).
4. U. Lakshminarayan, S. Ogrydiziak and H. L. Marcus, *1st Solid Free-Form Fabrication Symposium Proceedings*, Austin, TX, August 6–8, 16–26, 1990.
5. A. Lauder, M. J. Cima, E. Sachs and T. Fan, *Mater. Res. Soc. Symp. Proc.*, 249 331–336 (1992).
6. K. Pham-Gia, W. Rossner, B. Wessler, M. Schäfer and M. Schwarz, *cfi/Ber. DKG*, 83 [13] 36–40 (2006).
7. A. Licciulli, C. Esposito Corcione, A. Greco, V. Amicarelli and A. Maffezzoli, *J. Eur. Ceram. Soc.*, 24 [15–16] 3769–3777 (2004).
8. M. L. Griffith and J. W. Halloran, *J. Am. Ceram. Soc.*, 79 [10] 2601–2608 (1996).
9. de Hazan Y., M. Thanert, M. Trunec and J. Misak, *J. Eur. Ceram. Soc.*, 32 [6] 1187–1198 (2012).
10. R. Felzmann, *et al.*, *Adv. Eng. Mater.*, 14 [12] 1052–1058 (2012).
11. R. Lenk, A. Nagy, H.-J. Richter and A. Techel, *cfi/Ber. DKG*, 83 [13] 41–43 (2006).
12. P. Regenfuss, R. Ebert and H. Exner, *Laser Tech. J.*, 4 [1] 26–31 (2007).
13. Y.-C. Hagedorn, J. Wilkes, W. Meiners, K. Wissenbach and R. Poprawe, *Phys. Procedia*, 5 [B] 587–594 (2010).
14. Y. Wu, J. Du, K.-L. Choy and L. L. Hench, *J. Eur. Ceram. Soc.*, 27 [16] 4727–4735 (2007).
15. A. Gahler and J. G. Heinrich, *J. Am. Ceram. Soc.*, 89 [10] 3076–3080 (2006).
16. U. Gbureck, T. Hoelzel, I. Biermann, J. Barralet and L. M. Grover, *J. Mater. Sci. Mater. Med.*, 19 [4] 1559–1563 (2008).
17. H. Seitz, W. Rieder, S. Irsen, B. Leukers and C. Tille, *J. Biomed. Mater. Res. B Appl. Biomater.*, 74B [2] 782–788 (2005).
18. J. Y. S. Yoon, *et al., Int. J. Mat. Res.*, 103 [2] 200–206 (2012).
19. A. Khalyfa, W. Meyer, M. Schnabelrauch, S. Vogt and H.-J. Richter, *cfi/Ber. DKG*, 83 [13] 23–26 (2006).
20. U. Deisinger, F. Irlinger, R. Pelzer and G. Ziegler, *cfi/Ber. DKG*, 83 [13] 75–78 (2006).
21. R. Melcher, N. Travitzky, C. Zollfrank and P. Greil, *J. Mater. Sci.*, 46 [5] 1203–1210 (2011).
22. D. Polsakiewicz and W. Kollenberg, *refractories WORLDFORUM*, 4 [1] 1–8 (2012).
23. J. Günster, S. Engler and J. G. Heinrich, *Bull. Eur. Ceram. Soc.*, 1 25–28 (2003).
24. B. Cappi, E. Oezkol, J. Ebert and R. Telle, *J. Eur. Ceram. Soc.*, 28 [13] 2625–2628 (2008).
25. M. Allahverdi, S. C. Danforth, M. Jafari and A. Safari, *J. Eur. Ceram. Soc.*, 21 [10–11] 1485–1490 (2001).
26. S. Bose, J. Darsell, H. Hosick, L. Yang, D. K. Sarkar and A. Bandyopadhyay, *J. Mater. Sci. Mater. Med.*, 13 [1] 23–28 (2002).
27. T. Schlordt, S. Schwanke, F. Keppner, T. Fey, N. Travitzky and P. Greil, *J. Eur. Ceram. Soc.*, 33 [15–16] 3243–3248 (2013)
28. J. N. Stuecker, J. Cesarano III and D. A. Hirschfeld, *J. Mater. Process. Technol.*, 142 [2] 318–325 (2003).
29. K. Cai, *et al.*, *J. Am. Ceram. Soc.*, 95 [8] 2660–2666 (2012).
30. F. A. Cetinel, W. Bauer, M. Mueller, R. Knitter and J. Hausselt, *J. Eur. Ceram. Soc.*, 30 [6] 1391–1400 (2010).
31. R. Lenk and J. Adler, *J. Eur. Ceram. Soc.*, 17 [2–3] 197–202 (1997).
32. R. L. Coble, *J. Appl. Phys.*, 32 787 (1961).
33. S.-J. L. Kang, *Sintering—Densification, Grain Growth, and Microstructure*, Butterworth-Heinemann, Oxford, UK, 2005, ISBN: 978-0-7506-6385-4.
34. A. Petzold and J. Ulbricht, *Aluminiumoxid. Rohstoff – Werkstoff – Werkstoffkomponente*, Deutscher Verlag für Grundstoffindustrie GmbH, Leipzig, 1991, ISBN 3-342-00532-7.